

Article

Sunlight Bleaching of Subporphyrzine Dye Films

Vlad V. Travkin^{1,2,*}, Danila A. Semikov^{1,2}, Pavel A. Stuzhin² , Ivan A. Skvortsov² and Georgy L. Pakhomov^{1,2}

¹ Institute for Physics of Microstructures, Russian Academy of Sciences (IPM RAS), GSP-105, 603950 Nizhny Novgorod, Russia

² Organic Chemistry Department, Ivanovo State University of Chemistry and Technology (ISUCT), Sheremetyevsky Ave. 7, 153000 Ivanovo, Russia

* Correspondence: trav@ipmras.ru

Abstract: Stable subphthalocyanine-type dyes with a high electron affinity attract much attention as potential substitutes for traditional fullerenes in molecular electronics devices. One possible way to enhance the acceptor properties of the subphthalocyanine core is by replacing the peripheral benzene fragments (C_6H_4) with 1,2,5-thiadiazole fragments ($C_2N_2S_1$). However, the resistance of these materials to light or atmospheric effect remains an open question, which limits their further application in device manufacturing. In this work, we compare vacuum-deposited films of three derivatives, SubPzS₃H₀ (all peripheral fragments are 1,2,5-thiadiazoles), SubPzS₂H₄ (two fragments are 1,2,5-thiadiazoles and one fragment is benzene), and SubPcS₀H₁₂ (all benzenes, i.e., parent subphthalocyanine). Practically relevant substrates were used for deposition, namely, bare glass, glass/ITO or FTO, and PET/ITO. Photobleaching of films under continuous 1 sun illumination was studied in laboratory air, synthetic air, and ultrapure argon. It is shown that the exclusion of near-UV photons from the incident light spectrum, which corresponds to the absorption of subphthalocyanines in the Soret-band, strongly inhibits degradation. Absorption in the Q-band range initiates soft annealing rather than photobleaching of films. The stability of the films deposited on glass decreases as SubPzS₃H₀ > SubPzS₂H₄ > SubPcS₀H₁₂ in air, and vice versa in argon. The substrate adds more complexity to this picture. In argon, the ITO coating reduces degradation of all of the compounds equally, in contrast to the glass samples, while in air, the SubPzS₃H₀ films discolor completely. The latter reaction proceeds due to the indium-containing species migrating from the conductive coating.



Citation: Travkin, V.V.; Semikov, D.A.; Stuzhin, P.A.; Skvortsov, I.A.; Pakhomov, G.L. Sunlight Bleaching of Subporphyrzine Dye Films. *Appl. Sci.* **2023**, *13*, 1211. <https://doi.org/10.3390/app13021211>

Academic Editor: Joana F. B. Barata

Received: 15 December 2022

Revised: 12 January 2023

Accepted: 13 January 2023

Published: 16 January 2023



Copyright: © 2023 by the authors. Licensee MDPI, Basel, Switzerland. This article is an open access article distributed under the terms and conditions of the Creative Commons Attribution (CC BY) license (<https://creativecommons.org/licenses/by/4.0/>).

Keywords: photobleaching; subphthalocyanines; absorption spectra; thin films

1. Introduction

Subphthalocyanines and subporphyrzines (SubPc and SubPz) are tripyrrole-type dyes with tunable optical and redox properties that make them suitable candidates for use as nonfullerene acceptors in molecular electronics devices. In solutions, the interaction of molecules with the visible light has been studied quite well, including study on the photoexcited states, and their relaxation pathways [1–3]. In solids, however, the situation becomes intricate due to the intermolecular interactions, optical screening, or crystal-size effects.

Bender et al. [4] investigated the electronic structure of boron subphthalocyanine halide molecules using the density functional theory, DFT. They found that the nature of the axial ligand governs the stability of the macrocycle, while peripheral substituents rather affect the electrical and optical properties of the material. Nielsen et al. [5] examined the oxygen-dependent photophysics and photochemistry of subphthalocyanine derivatives and found out that the photosensitized production of a singlet molecular oxygen, $O_2(a^1\Delta_g)$, by these molecules is a key step in the degradation process. Furthermore, the addition of either β -carotene or astaxanthin as antioxidants inhibited degradation due to a combination of three processes. The first is deactivation of $O_2(a^1\Delta_g)$ to the oxygen ground state, $O_2(X^3\Sigma^-_g)$;

the second is quenching of the $O_2(a^1\Delta_g)$ precursor; the third is sacrificial reactions of the carotenoid with free radicals formed in the photo-initiated reactions. Troshin et al. [6] studied the light-induced degradation of various conjugated polymers deposited on glass, including those bearing thiophene and benzothiadiazole electron-accepting units. The photooxidation began even in the presence of trace amounts of oxygen, on the order of several hundreds of ppm, which is easier than in the case of polymers that contain more electron-deficient building blocks.

We have showed recently that the exposure of subphthalocyanine-based thin films to direct sunlight in air causes both chemical (photodestruction) and morphological (photoannealing) processes [7]. Yet, there are issues that need to be clarified. First, it is important to obviate the effect of destructive reactions with gas molecules from ambient [8] or with admixtures coming from the substrate or adjacent layers. Second, from the viewpoint of device stability [9], it is necessary to distinguish between the partial photodestruction of molecules and the soft annealing of the layer, as both processes are likely to arise under prolonged exposure of a sample to sunlight. Just thermal heating of a reference sample in the dark in order to reproduce solar exposure is not fully adequate [10], since the actual temperature up to which the irradiated molecular layer warms up is difficult to control, especially on a non-heat-conducting substrate [11,12]. Thirdly, it is interesting to know whether all wavelengths absorbed by a molecule initiate (or intensify) the destructive reaction, or only some of them. These issues are addressed here using tris (1,2,5-thiadiazolo) subporphyrinatoboron(III) chloride as a new molecular material for optoelectronics [13–15] and, for comparison, its derivatives with one or three benzene units (i.e., conventional subphthalocyaninato boron(III) chloride, SubPc)—Figure 1.

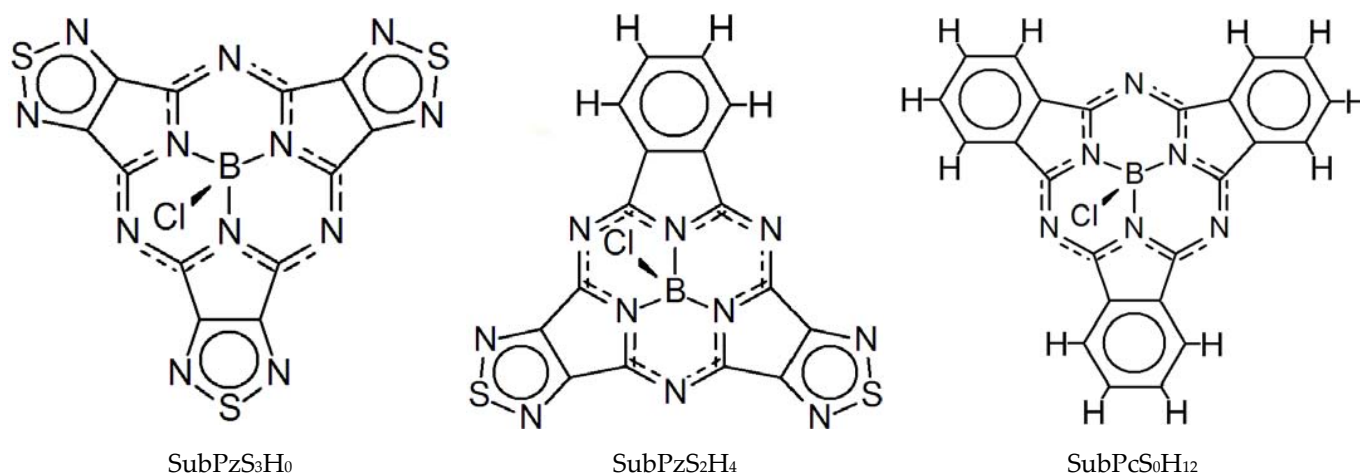


Figure 1. Molecular structures of compounds used in this work.

2. Experimental

The molecular structure of the compounds is shown in Figure 1. SubPzS₃H₀ and SubPzS₂H₄ were synthesized as described earlier [16], and SubPcS₀H₁₂ was supplied by Aldrich. Thin films were deposited in an upgraded VUP-5M vacuum evaporator at residual pressure $<3 \times 10^{-6}$ Torr. Three types of substrates highly functional in organic electronics were used: optical glass slides (K8), glass with ITO (10–25 Ohm/cm²) or FTO coating (7 Ohm/cm²), and polyethylene-terephthalate (PET) films with ITO coating (80 Ohm/cm²), all materials being Aldrich products. Bare glass slides were taken as a reference for the experiments with ITO/glass and FTO/glass. Transparent conductive oxides on solid (glass) and flexible (PET) substrates are of paramount importance in organic photovoltaic devices [17].

The nominal thickness of films was maintained at about 80 nm. The details of the deposition process and characterization of films can be found elsewhere [4,11,13–16,18]. The samples were exposed to an AM1.5 G illumination from a Zolix LCSS150A solar

simulator. Under direct (nonfiltered) illumination, the light power delivered to the sample was 100 mW/cm^2 , i.e., 1 sun. Optionally, a GS-12 long-pass filter (a 5 mm thick colored glass plate, analog of Newport FSQ-GG400) with a cut-on wavelength of 400 nm was used [10], which reduces the delivered light power to 78 mW/cm^2 . The light fell on the samples from the deposited organic film side rather than through the substrate. The exposition time was 12 h.

The films on substrates (5 samples of each type) were placed on a polished metal rod coated with black alkyd enamel to minimize the scattering of thermal radiation energy [11]. The temperature of the illuminated samples was monitored remotely using low-coherence tandem interferometry, a method originally developed at the IPM RAS [7,11,19]. Experiments were carried out in an Ar-filled glovebox ($<1 \text{ ppm O}_2, \text{H}_2\text{O}$), or in laboratory air at relative humidity in the range of 35–40%, or in dry synthetic air ($<0.5 \text{ ppm H}_2\text{O}$), at room temperature of 23–25 °C.

Electronic absorption spectra were recorded in the range of 340–900 nm using a Genesys 50 (ThermoFisher, Waltham, MA, USA) spectrometer with a 0.5 nm step. Deconvolution of the absorption bands was carried out in PeakFit v4.12 software (Systat) using the built-in algorithms based on Voigt functions with a sum-of-squares error (SSE) $<1\%$. The surface relief of subporphyrizin films was studied by atomic force microscopy, AFM (a CMM-2000 microscopy, Proton-MIET), white-light interferometry, WLI (a Talysurf CCI 2000 noncontact profilometer), and SEM (an Evo 10, Carl Zeiss scanning electron microscope). In certain cases (see further in the text), the film surface was decorated by depositing an ultrathin vanadium layer in an *e*-beam evaporator (AMOD, Angstrom Eng.). The X-ray diffraction analysis was performed using a Bruker D8 Discover diffractometer with Cu K α radiation ($\lambda = 0.154 \text{ nm}$) in the Bragg–Brentano and in the grazing incidence geometries.

3. Results and Discussion

3.1. Temperature Measurements

The temperature that a molecular layer is heated up to during irradiation was measured as a function of time [7,11,19], which is exemplified in Figure 2 for SubPzS₃H₀; other compounds showed similar profiles.

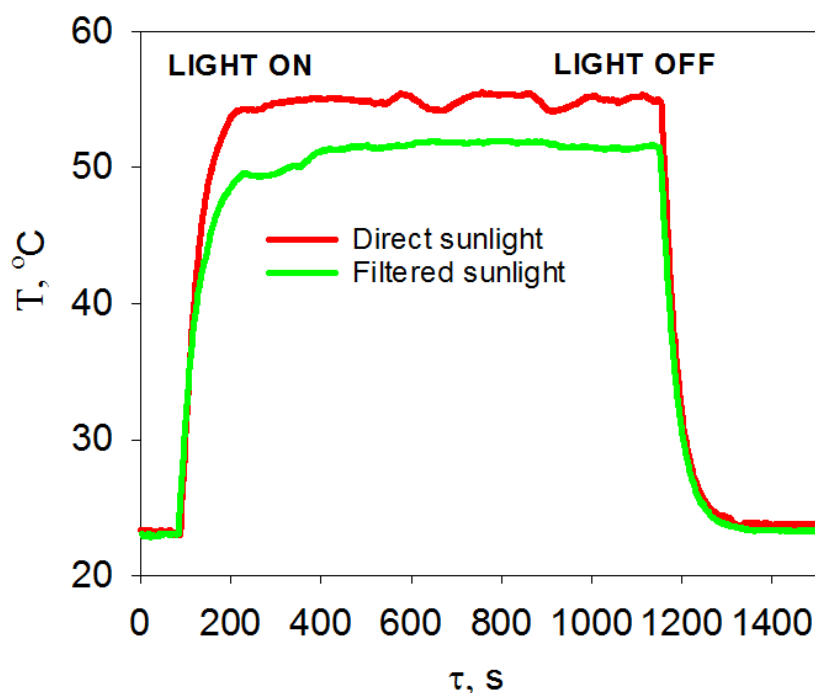


Figure 2. Temperature response of the SubPzS₃H₀ film on glass exposed to the direct (red curve) or filtered (green curve) 1-sun illumination in air.

In the first 250 s, the temperature of the 1-sun-illuminated film grew exponentially (see Figure S1 for details) up to 55 ± 2 °C, and then remained practically constant within instrumental fluctuations. After insertion of a GS-12 filter between the source and the sample (referred to as “filtered sunlight” hereinafter), about 400 s was required to reach the temperature plateau corresponding to 51 ± 1 °C—Figure 2. The warming-up to this range is not sufficient to cause the microscopic crystallization in the layer [20], but it can give rise to some morphological transformations [21] that can be regarded as ‘soft annealing’—see below.

3.2. Film Morphology

In both the θ -2 θ geometry and the grazing incidence angle geometries, all films under study showed no noticeable peaks in the X-ray diffraction patterns, regardless of whether they were pristine or irradiated. This indicates the absence of a measurable long-range order of molecules in the vacuum-deposited SubPc/SubPz layers. Moreover, in an attempt to stimulate crystallization in the SubPzS₃H₀ layer, the substrates were heated to 100 °C and above, similarly to what was performed in Ref [22] for SubPcS₀H₁₂. Despite this, the SubPzS₃H₀ layers retained their X-ray amorphous structure up to the resublimation threshold.

The surface of the SubPzS₃H₀ films was uniformly glossy to the eye, with a pinkish tinge typical of SubPc derivatives. The root-mean-square roughness (Sq) of the surface on a microscale was assessed by WLI with a pixel size of 1 μ m. Since the transparency of such films strongly reduces the reliability of WLI profiling, the film surface was decorated—see Experimental. Three random measurements on the sample surface were taken over the same scanning area; the averaged values are collected in Table 1.

Table 1. Values of Sq, in nm, for the V-metallized surface of SubPzS₃H₀ films on glass, measured over different scanning areas by WLI and AFM.

	Sample	Pristine	Direct Sunlight, Ar	Filtered Sunlight, Ar	Direct Sunlight, Air
Scanning area	0.9 × 0.9 cm ² (WLI)	5.8	2.0	4.4	4.9
	0.3 × 0.3 cm ² (WLI)	5.4	1.5	3.9	4.6
	0.1 × 0.1 cm ² (WLI)	5.4	0.8	3.8	4.3
	2.25 × 2.25 μ m ² (AFM)	17.7	11.8	19.4	17.5

The microscale surface relief revealed periodic height differences of no more than 20 nm—Figure S2. Microscopic Sq values in the range of 5–6 nm indicate that the 80 nm thick films were relatively smooth. Sq somewhat decreased with a decrease in scanning area, which correlates with a probability of coming across some large-sized inhomogeneities, including contaminations. After the exposure to unfiltered irradiation in argon, the films became about two times smoother, most of the spherical objects decreased in size. The filtered sunlight irradiation in both air and argon increased Sq only slightly—Table 1. Consequently, the film morphology on a microscale depends on the spectrum of the incident radiation rather than on atmosphere.

The combined AFM and SEM study added more detail to the surface morphology at the submicron scale—Figure 3; Table 1. The surface of the films, both in the pristine state and after irradiation, was covered with irregularly-shaped island-type objects of about 2 μ m in size. The lateral dimensions of such an object often exceeded the maximum area scanned with the tip, so that only its edge appeared in the AFM window—Figure 3a. The edge height was about 40 nm; these edges determined larger values of Sq derived from AFM—Table 1.

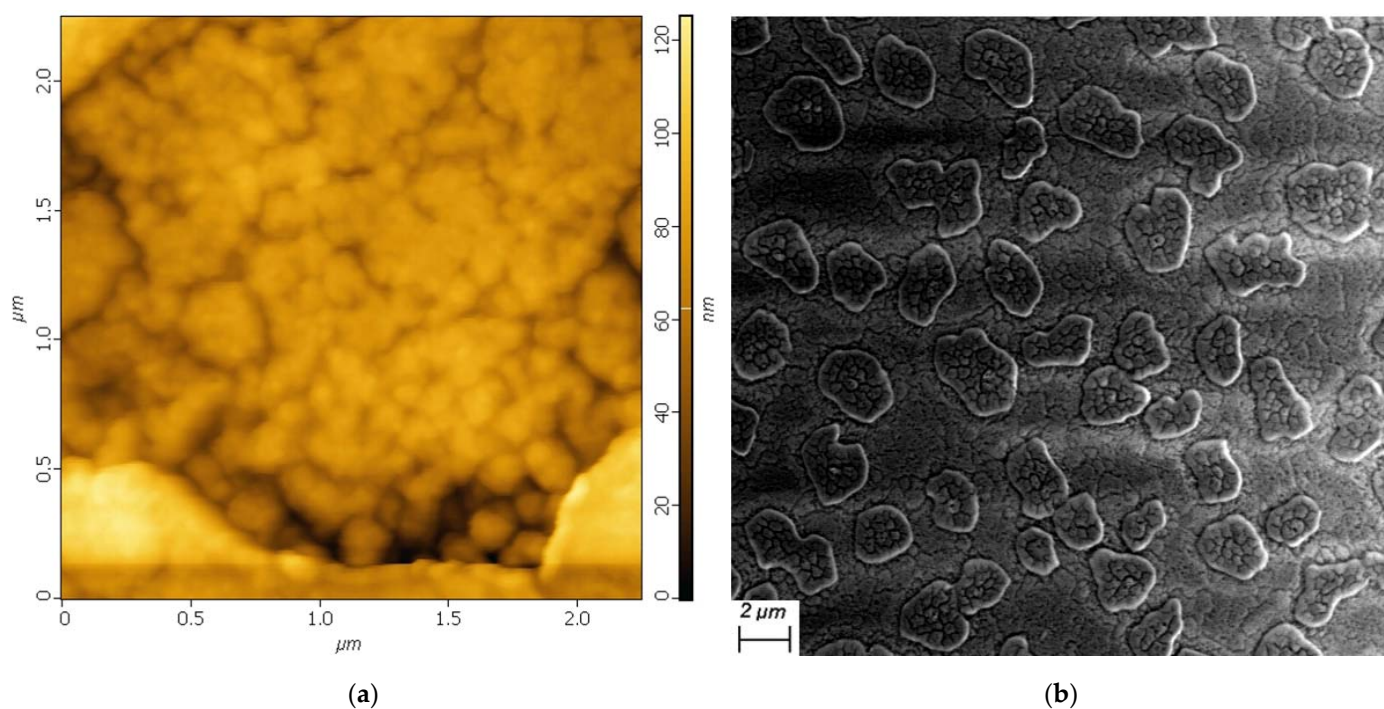


Figure 3. AFM image of the surface of pristine SubPzS₃H₀ film (V-metallized) in a scan window of $2.25 \times 2.25 \mu\text{m}^2$ (a), and SEM image of this surface in a window of $25 \times 25 \mu\text{m}^2$ (b, nonmetallized). The lower part of the AFM image displays the edge of a large surface object that is seen in SEM—inset.

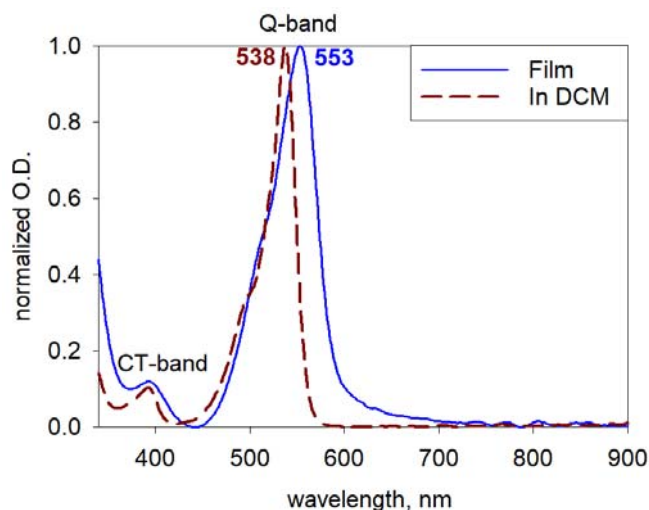
The observed objects cannot have resulted from V-decoration, since they also appeared on the nonmetallized surfaces, as seen by SEM—Figure 3b. SEM images confirm that the objects were flat, grainless, and resemble patches of dried soil rather than typically fractal nano-objects formed by vacuum-deposited phthalocyanines on glass or metal surfaces [23]. According to AFM, the surface of the islands and between them consisted of fine spherical structures of up to 100 nm in size—Figure 3a. The absence of faceting, or even a well-defined granular structure, of the objects suggests very low crystallinity [23]. There were also irregular ditches whose depth is comparable with the nominal film thickness. The prevailing heights in the AFM statistics (i.e., average film thickness) lie in the range of 70 nm.

Exposure to light did not cause any remarkable changes in the shape or concentration of the island-type objects, in whatever medium, with or without filter. Therefore, although some soft annealing of the films under continuous irradiation did take place (Figure S3), morphology transformation cannot be viewed as the dominant process affecting the optical density of films, which is discussed in the next sections.

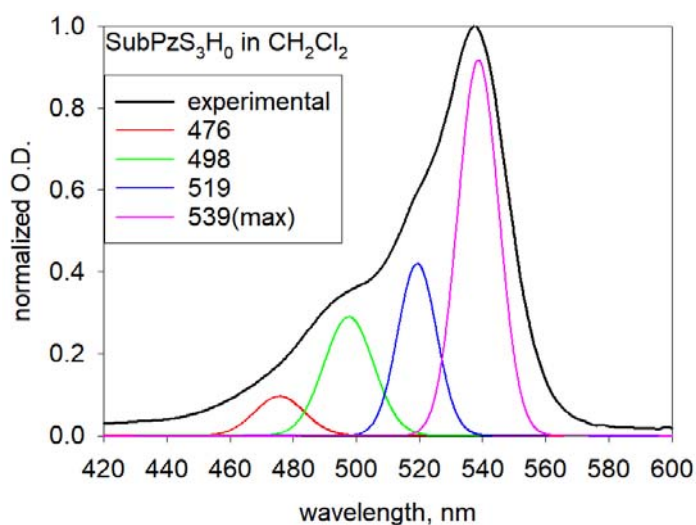
3.3. Absorption Spectra

As seen from Figure 1, SubPzS₃H₀ is a peripherally modified porphyrin dye without terminal hydrogen atoms. It can be treated as a subphthalocyanine derivative where all three benzene rings are replaced by the strongly electron-accepting thiazole rings [15]. This leads to a downward shift of the frontier molecular orbitals and to some widening of the optical bandgap [14,15,18]. The electronic absorption spectra of SubPzS₃H₀ consisted of two broad, intensive bands, Q- at 538 nm and B- (Soret) at 308 nm [16,18], and one less intensive band at ~390 nm (measured in DCM)—Figure 4. The latter band is absent in subphthalocyanines because it relates to the charge transfer (CT) from the π -system of subporphyrin chromophore to annulated 1,2,5-thiazole rings [18]. The most intensive Q-band located in the center of the visible range is assigned to the lowest-energy π - π^* transition ($2a_2 \rightarrow 1e^*$), i.e., corresponds to the HOMO-LUMO gap frequently used in the band diagrams of optoelectronic devices. The other intensive band, Soret-band, is composed of two transitions ($2a_1 \rightarrow 1e^*$ and $1a_1 \rightarrow 1e^*$) from HOMO-1 to the closely lying

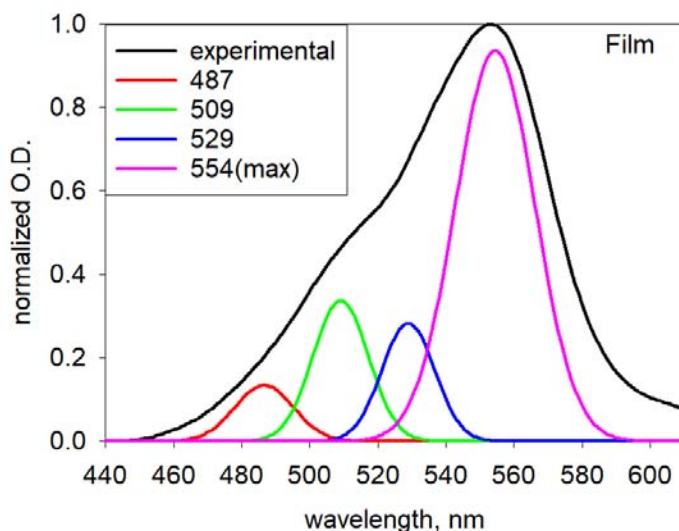
excited states B1 and B2 in the near-ultraviolet range [18]. In most devices, the photons reach or leave the photoactive molecular layer after passing through a substrate coated with a transparent electrode, glass/ITO for example. The substrate itself does not transmit light in the UV range; thus, the absorption spectra of films deposited on it become practically interesting at wavelengths longer than 320–340 nm (Figure S4).



(a)



(b)



(c)

Figure 4. (a) Absorption spectra of SubPzS₃H₀ dissolved in DCM and thin sublimed film on glass; deconvolution results for Q-band in solution (b) and film (c).

During aggregation, the bands broadened and shifted bathochromically compared to the spectrum of a diluted solution due to the intermolecular interactions [24,25]—Figure 4a. Judging from the low splitting and shift energies, the interaction between SubPzS₃H₀ molecules in a film is even weaker than it is in subphthalocyanines [4], which correlates with the X-ray data showing the absence of molecular ordering. Probably, this is associated with the lack of hydrogen bonding in SubPzS₃H₀, which can play an important role in a solid-state arrangement of subphthalocyanine molecules [26].

Figure 4b,c show the deconvolution results for the diffuse Q-band. The insertion of highly overlapping Gaussian peaks to deconvolve the experimental spectral profiles of phthalocyanines can give a virtually unlimited number of potentially successful fits and

is usually greeted with skepticism [27]. That is why here we do not strive here to achieve an ideal deconvolution procedure, but are just seeking to find a minimum admissible intraband composition and then trace its possible transformations in samples subjected to irradiation. As seen in Figure 4b, the Q-band for the SubPzS₃H₀ molecule in the dissolved state can be modelled by four Gaussian subpeaks, the main one being centered at 539 nm. Other subpeaks correspond to the vibronic satellites or may partly be due to the mixing between the singlet Q-state and the lowest triplet state [25]. The detailed identification of the vibronic structure, which is clearly seen in the experimental Q-band of SubPc/SubPz, based on theoretical spectra is still difficult [18].

In the film, the main subpeak in the Q-band shifted by 15 nm, and subpeaks at 476, 498 and 519 nm shifted by 10 nm (Figure 4c). The position of CT-band in the spectrum of SubPzS₃H₀ did not vary with aggregation. The effects of aggregation and remote exciton transfer on the vibrationally resolved absorption are theoretically considered in Ref. [25] for zinc phthalocyanine. It was shown that during the formation of aggregates, the vibrational features of Q-band smear out and their relative intensity ratio changes.

3.4. Photobleaching

3.4.1. On Bare Glass Substrate

The intensity of the strong Q-band, which basically accounts for the pink color of subphthalocyanine films, decreases after exposure to light, i.e., the films become bleached. The degree of bleaching in different conditions was quantified by measuring the ratio of the optical density at $\lambda_{\text{max}}^{\text{Q}}$ in the pristine and in the irradiated films of SubPzS₃H₀ ($D_{\text{pristine}}^{\text{Q}}/D_{\text{irradiated}}^{\text{Q}}$)—Table 1. The corresponding deconvolutions of the Q-band are shown in Figure S5. When the films were stored in the dark, they retained their color over the entire time of observation, regardless of the atmosphere.

The deconvolution results showed that the composition of the Q-band, including positions and relative intensities of subbands, did not change in the irradiated samples under any conditions, even when the Q-band intensity was reduced by a factor of two or more. The CT-band at 393 nm experienced a clear blue shift of 12 nm in the SubPzS₃H₀ films irradiated in air (Figure S6). This suggests an increase in the energy of the corresponding intramolecular transition, likely to be due to the interaction of the macrocycle with (oxidized?) decomposition products.

In some experiments, the samples were placed into a carefully purged cuvette filled with the so-called zero-gas, i.e., synthetic air prepared by mixing ultrapure oxygen and nitrogen in atmospheric proportions. We thereby minimized the influence of moisture, carbon oxides, and any kind of uncontrolled air components during irradiation; all other experimental conditions remained the same (the cuvette window attenuates the sunlight by about 10%). As seen from Table 2, the photobleaching of films under direct irradiation in synthetic air weakened, but did not cease completely. This result highlights the importance of controlling the laboratory atmosphere during measurements on thin-film samples [28,29]. Otherwise, the trends in the photo-assisted degradation of dye molecules may be misjudged.

Table 2. Maximum of Q-band ($\lambda_{\text{max}}^{\text{Q}}$) and ratio of the optical density at $\lambda_{\text{max}}^{\text{Q}}$ in pristine and irradiated SubPzS₃H₀ films on glass ($D_{\text{pristine}}^{\text{Q}}/D_{\text{irradiated}}^{\text{Q}}$).

	Pristine	Direct Sunlight in Air	Filtered Sunlight in Air	Direct Sunlight in Ar	Filtered Sunlight in Ar	Direct Sunlight in Synth. Air
$\lambda_{\text{max}}^{\text{Q}}, \text{nm}$	553	553	553	553	554	555
$D_{\text{pristine}}^{\text{Q}}/D_{\text{irradiated}}^{\text{Q}}$	-	1.6	1.2	2.2	1.2	1.4

As seen from Table 2, the photobleaching of SubPzS₃H₀ films on glass was deeper in argon than it was in air. This is somewhat unexpected [8], and one has to assume that

some of the atmospheric air components prevented the photoexcited state of SubPzS₃H₀ from further destruction. To prove this assumption, we conducted similar degradation tests with thin films of the two nearest analogs of SubPzS₃H₀, shown in Figure 1. The idea was to see if the chemical structure of the molecule, here, the presence of 1,2,5-thiadiazole units, is responsible for the resistance to photodestruction [6]. The absorption spectra of the films are shown in Figure 5a; the results are summarized in Table 3. As in solutions, there was a hypsochromic shift of the Q-band in the pristine films of SubPzS₃H₀ and SubPzS₂H₄ relative to the conventional SubPcS₀H₁₂. The reasons for these band shifts, as well as the redox behavior of these compounds, were considered in our previous studies [14,16,18].

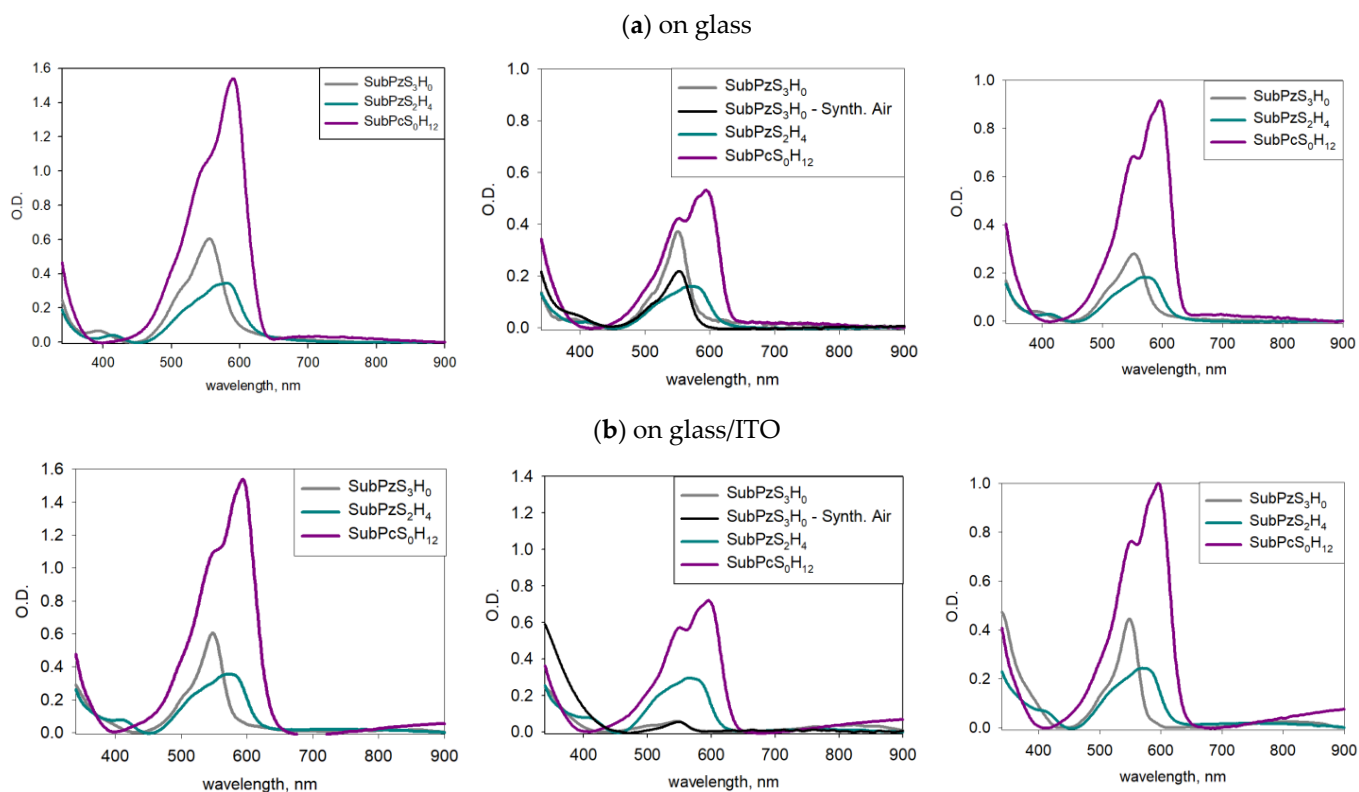


Figure 5. Absorption spectra of thin films of compounds in Figure 1 before (left) and after exposure to the direct sunlight in air (middle) and argon (right). The molecular structures of pigments are shown in Figure 1. (a) On glass; (b) On glass/ITO.

Table 3. Maximum of Q-band ($\lambda_{\text{max}}^{\text{Q}}$, nm) and ratio of the optical density at $\lambda_{\text{max}}^{\text{Q}}$ in pristine and direct-sunlight-irradiated films ($D_{\text{pristine}}^{\text{Q}}/D_{\text{irradiated}}^{\text{Q}}$) of three dyes (Figure 1) deposited on glass and glass/ITO substrates.

Dye	$\lambda_{\text{max}}^{\text{Q}}$, nm				$D_{\text{pristine}}^{\text{Q}}/D_{\text{irradiated}}^{\text{Q}}$				
	Pristine		Irradiated in Air		in Argon		in Synth. Air		
	glass	ITO	Glass	ITO	glass	ITO	Glass	ITO	ITO
SubPzS ₃ H ₀	553	548	553	546	1.6	10.2	2.2	1.4	10.1
SubPzS ₂ H ₄	581	570	569	565	2.1	1.2	2.0	1.4	1.2
SubPcS ₀ H ₁₂	590	594	596	596	3	2.1	1.7	1.4	2.4

blue for the wavelengths; red for the intensity change.

The replacement of one thiadiazole unit by a benzene ring reduces the stability of the SubPz molecule in air, while increasing it in argon (the films on bare glass). SubPzS₂H₄ is equally stable in both atmospheres and takes an intermediate position—Table 3. The films of “perhydrogenated” subphthalocyanine SubPcS₀H₁₂ are less resistant to irradiation in air than in inert atmosphere, which agrees with the trend noted earlier in Refs. [7,8,30].

Consequently, thiadiazole units, or rather, their intermediates with gas molecules, can stabilize the photoexcited state of the macroheterocycle.

Although photobleaching of films composed by SubPcS₀H₁₂ molecules is known ([7,8,21] and references therein), both the pathways and the end products of the reactions underlying this process appear to be not quite understood. It is clear that the end-products must be transparent in the visible range, and the most suitable candidate is phthalimide [7]. We examined this assumption in the following experiment. Solutions of SubPcS₀H₁₂ and phthalimide in DMSO (10⁻³ M) were prepared and placed in the quartz cuvettes. The cuvette with SubPcS₀H₁₂ was subjected to a xenon arc lamp irradiation with continuous argon purging until the solution became visually colorless. The UV/Vis spectra of phthalimide and thus bleached SubPcS₀H₁₂ solution were measured (Figure S7). In the latter case, a band at 291 nm was registered, which coincides with the pure phthalimide. Then, the bleached solution was evaporated, and the residue was collected and pressed into a KBr pellet. The FTIR spectra were measured and compared with the spectra of similar pellets containing neat SubPcS₀H₁₂ and phthalimide powders (Figure S7). In the spectrum of the residue, the characteristic stretching vibrations of NH- and B-OH groups at 3211 cm⁻¹, νC = O at 1740 cm⁻¹ and νB-O at 1384 cm⁻¹, were observed (Figure S7). It indicates, again, the presence of phthalimide, and, possibly, boric acid as reaction products.

However, the destruction of porphyrazines SubPzS₃H₀ and SubPzS₂H₄ may proceed in a different way, and yield different end products, such as (4H-pyrrolo[3,4-c][1,2,5]thiadiazole-4,6(5H)-dione)—Figure S7. However, the identification of the reaction scheme, as well as redox chemistry, is beyond the scope of this work.

UV filtering equally inhibits the photobleaching of SubPzS₃H₀ films in air and argon—Table 2. Filtered sunlight lacks the wavelengths responsible for the excitation of high-energy electronic transitions from HOMO-1 to LUMO in SubPc/SubPz (Figure S4). A 20% decrease in the Q-band intensity, observed in the spectra of films exposed to filtered irradiation, can be due to soft annealing of films rather than chemical destruction of molecules. As seen from Figure 2, the filtering itself does not prevent warming-up of a molecular film by incident light; the attenuation of the steady-state temperature is only 4–6 °C. When the subphthalocyanines were in a dissolved state where annealing effects were excluded, the photobleaching of solutions exposed to a filtered light was almost negligible, whereas without a filter, the Q-band intensity decreased noticeably (Figure S8). Hence, only the photons absorbed in the range of the Soret-band are responsible for the destructive reactions.

Turning to the comparison of differently substituted macroheterocycles from Figure 1, the fine structure of the Q-band in SubPzS₂H₄ and SubPcS₀H₁₂ films was weakly modified by irradiation in any atmosphere, similarly to SubPzS₃H₀ (Figure S9). The differences seen in Figure 5a concern only the overall intensity of the absorption curves, no new bands appear. This implies that the products of photodestruction are transparent in the range of 330–1000 nm also for the molecules bearing the benzene rings—Figures 1 and S7.

In order to check whether a certain amount of intact dye molecules survive in a visually discolored sample, after irradiation, substrate was flushed off the SubPzS₃H₀ film with DCM, and the spectrum of the obtained solution was compared with the spectrum of the original powder (before film deposition) dissolved in DCM. The spectra rigorously coincide, indicating that even a small amount of dye still resides in a heavily irradiated film in its intact form—Figure S10.

3.4.2. On Transparent Conductive Oxides (Glass/ITO, PET/ITO, Glass/FTO)

Generally speaking, the ITO (In₂O₃:SnO₂ = 90:10 wt%) coating on glass can be non-inert with respect to molecular film grown over it, albeit this circumstance is very seldom taken into account. There are two ways in which the substrate material can influence the overlying molecules. One is the so-called orientation effect that manifests itself in a specific arrangement of molecules in the first (and subsequent) layers of the growing film due to interaction with a substrate. The features of bulk molecular stacking determine optical

and other characteristics, including the color of dyes [31]. Since our films were relatively thick and disordered (see Section 3.2), this effect is unlikely. The other method involves the doping of the molecular layer with a very little amount of admixtures migrating from the substrate. Despite the inertness of the ITO coating and the gentleness of the thermal evaporation technique, such a conjecture has been proved valid by applying precise analytical techniques [29–31]. Unlike bare glass substrate, ITO coating contains oxidized indium and tin species, and their presence in a layer due to upward diffusion could trigger the photolysis of dye molecules.

First of all, the spectra of the pristine SubPc/SubPz films deposited on bare glass and on ITO do not completely coincide—Figure 5. In the SubPzS₃H₀ films deposited on ITO, the red edge of the Soret-band broadens and the CT-band transforms into a shoulder of the Soret-band by moving to the left and decreasing in intensity (details in Figure S11). A similar, but less pronounced trend was demonstrated by SubPzS₂H₄. SubPcS₀H₁₂ is not sensitive to the substrate material. At this moment, we have no explanation for such spectral profiles.

Secondly, the photobleaching also depends on whether the film was deposited on bare glass or on ITO—Table 3. Each compound has its own peculiarities of interaction with light/air/substrate—Figure 5. The most dramatic destruction occurred with SubPzS₃H₀ on ITO. After irradiation in laboratory or synthetic air, the SubPzS₃H₀ films on ITO lost their original color and became almost transparent. For the other two compounds, the ITO underlayer had a rather stabilizing effect. In argon, this stabilizing effect ensures the same degree of photobleaching for all compounds.

Despite such a strong photobleaching effect of SubPzS₃H₀ films on ITO in air, their absorption spectrum, again, did not change fundamentally. This indicates that surviving dye molecules retained the original structure of their chromophores, and the end-products of destruction were mostly transparent or highly volatile. Nonetheless, a closer look reveals some distinct spectral features. First, there appeared a new component at the red side of the diffuse Q-band (580–600 nm) in the spectra of irradiated SubPzS₃H₀ films—Figure S12. It could be an artifact of the fitting procedure, but, as we will show further, this is unlikely to be the case. Secondly, we noticed that the relative intensity of all subbands composing the Q-band increased in the films after irradiation (Table S1). As said above, the nearest-neighbor exciton coupling in the condensed state of zinc phthalocyanine was analyzed in Ref. [25], and the authors arrived at an important conclusion that an increase in the length of molecular aggregates leads to a decrease in the intensity of high-energy subpeaks in the vibrationally resolved Q-band spectrum. Conversely, growing blue subpeaks indicate shortening of the aggregation chain. Applying this model to our system and assuming that short-range molecular aggregates actually exist in an intact film, we do see that photobleaching destroys the ordering of molecules of any compound deposited on a glass/ITO substrate. This might be explained by the partial “dissolving” of intact dye molecules in the end-products of the destruction reaction.

Next, we examined the photodestruction in the SubPzS₃H₀ films deposited on PET/ITO substrates, where the bulk support under the conductive indium tin oxide coating is polymeric—Figure 6. Here, the Q-band was composed of five subbands (Figure S13). The fifth component arose at the longwave shoulder at around 613 nm, similar to what was observed in the SubPzS₃H₀ films on glass/ITO irradiated in air. This new subband tended to grow in the samples exposed to sunlight.

The photobleaching of SubPzS₃H₀ films on PET/ITO was even more severe than in the case of a glass/ITO substrate—Figure 6a. The $D^Q_{\text{pristine}}/D^Q_{\text{irradiated}}$ ratio was 12.2 and 3.0 for the films irradiated in air and in argon, respectively—cf. Table 3. We tentatively assume that the release of indium-containing species from the conductive layer made on the porous and flexible organic support could proceed more easily. The diffusion of chemically active organic admixtures from the PET substrate through a thick ITO coating towards the subporphyrazine layer is less realistic.

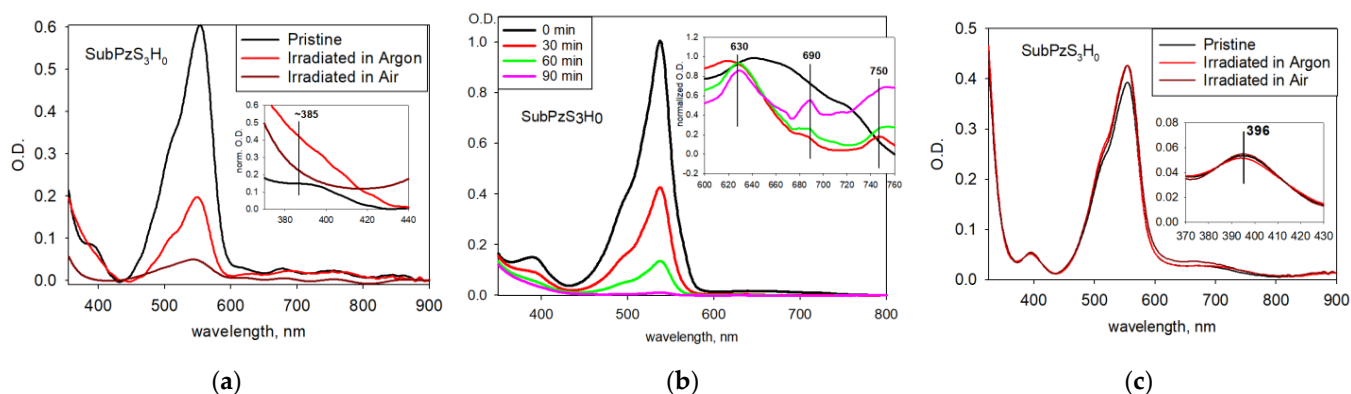


Figure 6. Spectra of SubPzS₃H₀ films on PET/ITO substrate before and after direct sunlight irradiation either in air or in argon (a); Time-resolved absorption spectra of SubPzS₃H₀ solution in acetone in presence of In(Acac)₃ before (black) and after (red, green, pink) direct illumination in argon (inset—normalized 600–760 nm region) (b); Spectra of SubPzS₃H₀ films on glass/FTO substrate before and after direct sunlight irradiation either in air or in argon, inset—the area of the CT-band (c).

The following experiment was carried out to clear up the effect of indium-containing species. SubPzS₃H₀ was dissolved in dehydrated high-purity acetone with and without a pre-added equimolar (10^{-5} M) quantity of indium acetylacetonate, In(Acac)₃, in a 10 mm quartz cuvette. As known, In(Acac)₃ can serve as a precursor for the fabrication of ITO by the CVD process [32]. In this way, we attempted to imitate, very roughly, of course, a reaction between the indium ion and the dye molecule. The spectra of the mixed SubPzS₃H₀:In(Acac)₃ solution were recorded as a function of time in the dark and under illumination within 6 h under continuous argon purging.

Photobleaching of the irradiated SubPzS₃H₀ solution with the indium content occurred 15% faster than in the control sample without In(Acac)₃. Furthermore, three low-intensity bands clearly appeared in the range of 620–760 nm in place of the initial blurry arc, and their intensity grew with the irradiation time—Figure 6b. These bands may indicate the reduction/tetramerization processes associated with the formation of trace amounts of indium tetrakis(thiadiazole)porphyrazine or phthalocyanine complexes (Figure S7c) [33]. In the case of a SubPcS₀H₁₂:In(Acac)₃ solution prepared and treated in similar conditions, the intensity of the Q-band did not differ for solutions with or without indium. In this case, there appeared only one low-intensity band at 650 nm (Figure S7c).

Chemical reactions with subphthalocyanine and its derivatives usually proceed through cleavage of the halogen axial ligand due to high lability of the B-Cl bond [4,34] (Figure S7). From theoretical considerations [4], the farther the electron density is shifted from the heterocycle to the periphery, the lower the B-Cl bond energy is. Therefore, the detachment of chlorine in the axial position will proceed easier in SubPcS₃H₀ than in SubPcS₀H₁₂.

Experiments with solutions help visualize intermediates or colored reaction products that cannot be registered in thin-film samples due to (i) a very small amount of the reagent (In) and (ii) a growing absorption tail in the long-wavelength region for samples on a glass/ITO substrate—cf. Figure 5b.

Note that the degree of photobleaching of SubPc/SubPz was practically independent of whether it occurred in atmospheric (i.e., relatively humid) or synthetic (dry) air—Table 3, Figure 5. Therefore, the destruction reaction involves oxygen, being less sensitive to other ambient air components.

To further elucidate the role of indium-containing species coming from the substrate [35] in facilitating the light-assisted destruction of SubPzS₃H₀, the experiments were repeated with SubPzS₃H₀ films deposited on glass/FTO substrates, where FTO is a fluorine-doped tin dioxide, SnO₂:F. The photobleaching of films on indium-free substrates did not occur, either in air or in argon—Figure 6c. On the contrary, the Q-band intensity even slightly increased, possibly due to the morphological transformation in the layer. This

corroborates the above assumption on the principal role of indium-containing species in accelerating the photobleaching of SubPzS₃H₀ films.

4. Conclusions

(a) The degree of bleaching of SubPz/SubPc thin films exposed to sunlight strongly depends on the environment. While it was intuitively anticipated that the light-driven reactions would run differently in ambient air and in inert gas, the substrate effect was unsuspected.

(b) The impact of air can be dammed by varying the composition of peripheral rings in a subphthalocyanine molecule. Parent SubPcS₀H₁₂ subphthalocyanine discolors deeply in air but is more stable in argon, whereas for SubPzS₃H₀, the situation is reversed. These observations are valid for films deposited on bare glass.

(c) ITO coating on glass generally inhibits photobleaching. The exception is a SubPzS₃H₀ film irradiated in the presence of oxygen, in which the Q-band intensity drops nearly 10-fold, i.e., the films become almost transparent. By further replacing the substrates with PET/ITO and glass/FTO, we confirmed that namely ITO components are responsible for this anomaly. Presumably, the accelerated bleaching of SubPzS₃H₀ films on ITO results from a specific reaction of symmetrical subporphyrine macroligand in its photoexcited state with O₂ in the presence of (catalyzed by?) indium-containing species coming from the conductive coating.

(d) If near-UV photons are removed from the incident light by application of a long-pass filter cutting $\lambda < 400$ nm, then the spectrum of irradiated films changes only slightly. A slight change after UV-free irradiation is basically due to the solid-state processes, such as annealing-induced morphological transformation. In addition, some photoactivated reactions with residual atmospheric components and/or with admixtures emerging from the substrate cannot be ruled out.

(e) Therefore, photo(catalytic?) destruction of the subphthalocyanine chromophore is effective only when high-energy electronic transitions in the dye molecule corresponding to the Soret-band range are involved. This finding can potentially be useful in the design or selection of phthalocyanine-based materials for thin-film electronic devices, where photostability is an important issue. For instance, the macroheterocycles having blue-shifted Soret-band would be interesting in photovoltaics, since the destructive UV component of sunlight will naturally be filtered by the substrate through which the light enters the device.

Supplementary Materials: The following supporting information can be downloaded at <https://www.mdpi.com/article/10.3390/app13021211/s1>: Figure S1. Initial sections of the ‘temperature vs. time’ dependence: (a) light-On and (b) light-Off (direct sunlight). Rsqr—correlation coefficient; Figure S2. Cross-sectional profiles and 3D surface maps of V-metallized SubPzS₃H₀ films on glass, scanning area 0.3 × 0.3 mm²: pristine film (a) and films irradiated by the direct sunlight in Ar (b), filtered sunlight in Ar (c), and filtered sunlight in air (d); Figure S3. Height distribution (top panels) and 2D images (bottom panels) of V-metallized SubPzS₃H₀ films on glass: pristine film (a) and films irradiated by the direct sunlight in Ar (b), filtered sunlight in Ar (c), and filtered sunlight in air (d); Figure S4. (a) Absorption spectrum of the SubPzS₃H₀ film in the UV/Vis/NIR range and transmission of the glass/ITO substrate (red dashed line). (b) Absorption spectrum of the SubPzS₃H₀ film from Figure 4a and transmission of the GS-12 optical filter in the visible/NIR range. Filter cuts off the wavelengths <400 nm, while in the area of Q-band, its transparency is better than 90%. The AM1.5 G simulated sunlight has a shortwave limit at ~300 nm; Figure S5. Deconvolution of the Q-band in the spectrum of the SubPzS₃H₀ film on glass exposed to direct (a) and filtered (b) sunlight in air; direct (c) and filtered sunlight in argon (d); direct sunlight in synthetic air (e); Figure S6. Normalized absorption spectra of SubPzS₃H₀ (a,b) and SubPzS₂H₄ (c,d) films: before (black curves) and after exposure to the filtered (solid green curves) or direct (dotted green curves) sunlight in air (a) and argon (b), all on glass substrate; before (black curves) and after exposure to the direct sunlight in air (red curves) and argon (dark red curves)—on glass (c) and on ITO (d) substrate; Figure S7. (a) Scheme of photodestruction of SubPc/SubPz induced by UV light (tentative) and possible tetramerization. (b) FTIR spectra of SubPcS₀H₁₂, decomposition product and phthalimide in the KBr pellets (left); UV/Vis spectra of decomposition product and phthalimide in the DMSO solution (right). (c) Time-resolved UV/Vis

spectra of SubPzS₀H₁₂ solution in acetone in the presence of In(Acac)₃ before (black) and after (red, green, pink) direct illumination in argon (inset—600–760 nm region, normalized); Figure S8. Spectra of SubPcS₃H₀ (a,b) and SubPcS₀H₁₂ (c,d) solutions in acetone before and after irradiation during 2 h without and with the UV filter and without (a,c) or with (b,d) In(acac)₃; Figure S9.I. Deconvolution of Q-band in the spectrum of SubPzS₂H₄ film on glass: initial (a) and exposed to direct sunlight in air (b) and in argon (c); Figure S9.II. Deconvolution of Q-band in the spectrum of SubPcS₀H₁₂ film on glass: initial (a) and exposed to direct sunlight in air (b) and in argon (c); Figure S10. Comparison of spectra of freshly made SubPzS₃H₀ solution in DCM (dashed), film after irradiation treatment in air (dotted), and the solution made by flashing this film back into DCM; Figure S11. Absorption spectra of films deposited on various substrates: (a) SubPzS₃H₀, (b) SubPzS₂H₄, (c) SubPcS₀H₁₂; Figure S12.I. Deconvolution of Q-band in the spectrum of SubPzS₃H₀ film on glass/ITO initial (a) and exposed to direct sunlight: in air (b), in argon (c), in synthetic air (d); comparison of all spectra (e); Figure S12.II. Deconvolution of Q-band in the spectrum of SubPzS₂H₄ film on glass/ITO initial (a) and exposed to direct sunlight: in air (b), in argon (c), in synthetic air (d); comparison of all spectra (e); Figure S12.III. Deconvolution of Q-band in the spectrum of SubPcS₀H₁₂ film on glass/ITO initial (a) and exposed to direct sunlight: in air (b), in argon (c), in synthetic air (d); comparison of all spectra (e); Table S1. The relative intensities of subpeaks according to the deconvolution results in Figures S5, S9, S12 and S13; Figure S13. Deconvolution of Q-band in the spectrum of SubPzS₃H₀ film on PET/ITO initial (a) and exposed to direct sunlight: in air (b), in argon (c).

Author Contributions: V.V.T., D.A.S., P.A.S., I.A.S. and G.L.P. contributed to the study conception and design. Synthesis and characterization of SubPzS₃H₀ and SubPzS₂H₄ were performed under supervision of P.A.S. Thin films were obtained and characterized by V.V.T. The temperature measurements were made by D.A.S. The draft was written by G.L.P. The authors commented on all versions of the manuscript. All authors have read and agreed to the published version of the manuscript.

Funding: This work is supported by the Center of Excellence «Center of Photonics», funded by The Ministry of Science and Higher Education of the Russian Federation, contract No. 075-15-2020-906.

Informed Consent Statement: Not applicable.

Data Availability Statement: The data obtained and/or analyzed during the current study are available from the corresponding author on reasonable request.

Conflicts of Interest: The authors have no relevant financial or nonfinancial interest to disclose.

References

1. Lavarda, G.; Labella, J.; Victoria Martinez-Diaz, M.; Salome Rodriguez-Morgade, M.; Osuka, A.; Torres, T. Recent advances in subphthalocyanines and related subporphyrinoids. *Chem. Soc. Rev.* **2022**, *51*, 9482–9619. [[CrossRef](#)]
2. Dowds, M.; Nielsen, M.B. Controlling the optical properties of boron subphthalocyanines and their analogues. *Mol. Syst. Des. Eng.* **2021**, *6*, 6–24. [[CrossRef](#)]
3. Zhang, X.; Tang, Y.; Yang, K.; Chen, P.; Guo, X. Additive-free non-fullerene organic solar cells. *ChemElectroChem.* **2019**, *6*, 5547–5562. [[CrossRef](#)]
4. Hildebrand, M.; Holst, D.; Bender, T.; Kronik, L. Electronic structure, bonding, and stability of boron subphthalocyanine halides and pseudohalides. *Adv. Theory Simul.* **2022**, *5*, 2100400. [[CrossRef](#)]
5. Bregnhøj, M.; Prete, M.; Turkovic, V.; Petersen, A.U.; Nielsen, M.B.; Madsen, M.; Ogilby, P.R. Oxygen-dependent photophysics and photochemistry of prototypical compounds for organic photovoltaics: Inhibiting degradation initiated by singlet oxygen at a molecular level. *Methods Appl. Fluoresc.* **2011**, *8*, 014001. [[CrossRef](#)] [[PubMed](#)]
6. Martynov, I.V.; Inasaridze, L.N.; Troshin, P.A. Resist or oxidize: Identifying molecular structure–photostability relationships for conjugated polymers used in organic solar cells. *ChemSusChem.* **2022**, *15*, e202101336. [[CrossRef](#)]
7. Pakhomov, G.L.; Travkin, V.V.; Drozdov, M.N.; Sachkov, Y.I.; Yunin, P.A. Small-molecule heterojunctions: Stability to ageing under sunlight. *Appl. Surf. Sci.* **2022**, *578*, 152084. [[CrossRef](#)]
8. Burlingame, Q.; Tong, X.; Hankett, J.; Sloatsky, M.; Chen, Z.; Forrest, S.R. Photochemical origins of burn-in degradation in small molecular weight organic photovoltaic cells. *Energy Environ. Sci.* **2015**, *8*, 1005–1010. [[CrossRef](#)]
9. Grant, T.M.; Josey, D.S.; Sampson, K.L.; Mudigonda, T.; Bender, T.P.; Lessard, B.H. Boron subphthalocyanines and silicon phthalocyanines for use as active materials in organic photovoltaics. *Chem. Rec.* **2019**, *19*, 1093–1112. [[CrossRef](#)]
10. Li, Y.; Huang, X.; Ding, K.; Sheriff, H.K.M.; Ye, L.; Liu, H.; Li, C.-Z.; Ade, H.; Forrest, S.R. Non-fullerene acceptor organic photovoltaics with intrinsic operational lifetimes over 30 years. *Nat. Commun.* **2021**, *12*, 5419. [[CrossRef](#)]
11. Travkin, V.V.; Koptyaev, A.I.; Pakhomov, G.L.; Volkov, P.V.; Semikov, D.A.; Luk'yanov, A.Y. Experimental study of heat transfer in thin-film perovskite-based structures using a low-coherent tandem interferometry. *Tech. Phys. Lett.* **2021**, *23*, 31. [[CrossRef](#)]

12. Burlafinger, K.; Strohm, S.; Joisten, C.; Woiton, M.; Classen, A.; Hepp, J.; Heumüller, T.; Brabec, C.J.; Vetter, A. Accelerated lifetime testing of thin-film solar cells at high irradiances and controlled temperatures. *Prog. Photovolt. Res. Appl* **2022**, *30*, 518–527. [[CrossRef](#)]
13. Travkin, V.; Koptyaev, A.; Hamdoush, M.; Pakhomov, G. Molecular optical filtering in perovskite solar cells. *J Mater. Sci. Mater. Electron.* **2022**, *33*, 7728–7737. [[CrossRef](#)]
14. Pakhomov, G.L.; Travkin, V.V.; Khamdoush, M.; Zhabanov, Y.A.; Stuzhin, P.A. Thiadiazole fused subporphyrines as acceptors in organic photovoltaic cells. *Macromolecules* **2017**, *10*, 548–551. [[CrossRef](#)]
15. Skvortsov, I.A.; Kovkova, U.P.; Zhabanov, Y.A.; Khodov, I.A.; Somov, N.V.; Pakhomov, G.L.; Stuzhin, P.A. Subphthalocyanine-type dye with enhanced electron affinity: Effect of combined azasubstitution and peripheral chlorination. *Dyes Pigm.* **2021**, *185*, 108944. [[CrossRef](#)]
16. Hamdoush, M.; Ivanova, S.S.; Pakhomov, G.L.; Stuzhin, P.A. Heterocyclic subphthalocyanine analogue—Boron(III) subporphyrine with fused 1,2,5-thiadiazole rings. *Macromolecules* **2016**, *9*, 230–233. [[CrossRef](#)]
17. Afre, R.A.; Sharma, N.; Sharon, M.; Sharon, M. Transparent conducting oxide films for various applications: A review. *Rev. Adv. Mater. Sci.* **2018**, *53*, 79–89. [[CrossRef](#)]
18. Hamdoush, M.; Nikitin, K.; Skvortsov, I.; Somov, N.; Zhabanov, Y.; Stuzhin, P.A. Influence of heteroatom substitution in benzene rings on structural features and spectral properties of subphthalocyanine dyes. *Dyes Pigm.* **2019**, *170*, 107584. [[CrossRef](#)]
19. Volkov, P.; Semikov, D.; Goryunov, A.; Luk'yanov, A.; Tertyshnik, A.; Vopilkin, E.; Krayev, S. Miniature fiber-optic sensor based on Si microresonator for absolute temperature measurements. *Sens. Actuator A Phys.* **2020**, *316*, 112385. [[CrossRef](#)]
20. Wang, J.; Yang, P.; Zhao, X.; Yang, L. Boron subphthalocyanine chloride crystalline thin film with a long range exciton diffusion length grown assisted by negative surface charges. *Thin Solid Films* **2017**, *636*, 527–531. [[CrossRef](#)]
21. Wang, N.; Tong, X.; Burlingame, Q.; Yu, J.; Forrest, S.R. Photodegradation of small-molecule organic photovoltaics. *Sol. Energy Mater. Sol. Cells* **2014**, *125*, 170–175. [[CrossRef](#)]
22. Son, Y.H.; Kim, G.W.; Jeon, W.S.; Pode, R.; Kwon, J.H. Thermal annealing effect of subphthalocyanine (SubPc) donor material in organic solar cells. *Mol. Cryst. Liq. Cryst.* **2012**, *565*, 8–13. [[CrossRef](#)]
23. Karan, S.; Mallik, B. Templating effects and optical characterization of copper (II) phthalocyanine nanocrystallites thin film: nanoparticles, nanoflowers, nanocabbages, and nanoribbons. *J. Phys. Chem. C* **2007**, *111*, 7352–7365. [[CrossRef](#)]
24. Chen, X.; Zheng, S. Inferring the molecular arrangements of boron subphthalocyanine chloride in thin film from a DFT/TDDFT study of molecular clusters and experimental electronic absorption spectra. *Org. Electron.* **2018**, *62*, 667–675. [[CrossRef](#)]
25. Feng, S.; Wang, Y.-C.; Liang, W.Z.; Zhao, Y. Vibrationally resolved absorption spectra and exciton dynamics in zinc phthalocyanine aggregates: Effects of aggregation lengths and remote exciton transfer. *J. Phys. Chem. A* **2021**, *125*, 2932–2943. [[CrossRef](#)]
26. Virido, J.D.; Crandall, L.; Dang, J.D.; Fulford, M.V.; Lough, A.J.; Durfee, W.S.; Bender, T.P. The influence of strong and weak hydrogen bonds on the solid state arrangement of hydroxy-containing boron subphthalocyanines. *CrystEngComm* **2013**, *15*, 8578–8586. [[CrossRef](#)]
27. Mack, J.; Stillman, M.J. Assignment of the optical spectra of metal phthalocyanines through spectral band deconvolution analysis and ZINDO calculations. *Coord. Chem. Rev.* **2001**, *219–221*, 993–1032. [[CrossRef](#)]
28. Muckley, E.S.; Miller, N.; Jacobs, C.B.; Gredig, T.; Ivanov, I.N. Morphology-defined interaction of copper phthalocyanine with O₂/H₂O. *J. Photon. Energy* **2016**, *6*, 045501. [[CrossRef](#)]
29. Jørgensen, M.; Norrman, K.; Krebs, F.C. Stability/degradation of polymer solar cells. *Sol. Energy Mater. Sol. Cells* **2008**, *92*, 686–714. [[CrossRef](#)]
30. Pakhomov, G.L.; Drozdov, M.N.; Travkin, V.V.; Lopatin, M.A.; Shashkin, V.I. Reversal of rectification in fullerene-based devices. *Synth. Met.* **2014**, *195*, 91–96. [[CrossRef](#)]
31. Lincke, G. Molecular stacks as a common characteristic in the crystal lattice of organic pigment dyes A contribution to the “soluble–insoluble” dichotomy of dyes and pigments from the technological point of view. *Dyes Pigm.* **2003**, *59*, 1–24. [[CrossRef](#)]
32. Szkutnik, P.D.; Roussel, H.; Lahootun, V.; Mescot, X.; Weiss, F.; Jiménez, C. Study of the functional properties of ITO grown by metalorganic chemical vapor deposition from different indium and tin precursors. *J. Alloys Compd.* **2014**, *603*, 268–273. [[CrossRef](#)]
33. Donzello, M.P.; Agostinetto, R.; Ivanova, S.S.; Fujimori, M.; Suzuki, Y.; Yoshikawa, H.; Shen, J.; Awaga, K.; Ercolani, C.; Kadish, K.M.; et al. Tetrakis(thiadiazole)porphyrines. 4. Direct template synthesis, structure, general physicochemical behavior, and redox properties of AlIII, GaIII, and InIII complexes. *Inorg. Chem.* **2005**, *44*, 8539–8551. [[CrossRef](#)] [[PubMed](#)]
34. Guilleme, J.; González-Rodríguez, D.; Torres, T. Triflate-subphthalocyanines: Versatile, reactive intermediates for axial functionalization at the boron atom. *Angew. Chem. Int. Ed.* **2011**, *50*, 3506–3509. [[CrossRef](#)] [[PubMed](#)]
35. Sharma, A.; Andersson, G.; Lewis, D.A. Role of humidity on indium and tin migration in organic photovoltaic devices. *Phys. Chem. Chem. Phys.* **2011**, *13*, 4381–4387. [[CrossRef](#)]

Disclaimer/Publisher's Note: The statements, opinions and data contained in all publications are solely those of the individual author(s) and contributor(s) and not of MDPI and/or the editor(s). MDPI and/or the editor(s) disclaim responsibility for any injury to people or property resulting from any ideas, methods, instructions or products referred to in the content.